ScienceDirect

Contents lists available at ScienceDirect

Journal of Iron and Steel Research, International

journal homepage: www.chinamet.cn

Hot tearing susceptibility of Fe-20.96Cr-2.13Ni-0.15N-4.76Mn-0.01Mo duplex stainless steel

Zhi-qiang Wei, Xiang-ru Chen*, Hong-gang Zhong, Qi-jie Zhai, Gang Wang

State Key Laboratory of Advanced Special Steel & Shanghai Key Laboratory of Advanced Ferrometallurgy & School of Materials Science and Engineering, Shanghai University, Shanghai 200072, China

ARTICLE INFO

Key words:
Duplex stainless steel
Hot tearing
Solidification
Contraction stress
Core temperature

ABSTRACT

The hot tearing susceptibility of a Fe-20.96Cr-2.13Ni-0.15N-4.76Mn-0.01Mo duplex stainless steel was investigated using method of constrained solidification shrinkage in one dimension. An apparatus for real-time measuring the contraction stress and temperature during solidification was developed, which can achieve the in-situ observation of melting and solidification and avoid the large temperature gradient of casting under the condition of pouring. The results show that the contraction stress increases significantly when the core temperature of casting reaches the liquidus temperature. The contraction stress is released when the core temperature of casting reaches 1456 ℃. At this temperature, the hot tearing susceptibility of duplex stainless steel is the largest. With decreasing the core temperature to 1363 ℃, the slope of contraction stress increases, which is related to the ferrite-to-austenite transformation.

1. Introduction

Duplex stainless steel (DSS) is a stainless steel composed of ferritic phase and austenitic phase, in which the austenite accounts for 30% to 50%. DSS inherits some advantages from both ferritic stainless steel and austenitic stainless steel through the component optimization and thermal treatment[1]. Owing to its good mechanical properties and excellent corrosion resistance, DSS, as an important structural material, is widely used in the industries of petro-chemistry and ship building[2,3]. However, DSS is susceptible to hot tearing defects during the processes of solidification and/or welding because these processes bring about a broad temperature range for the solidification of molten steels with an insufficient fluidity[4].

Hot tearing occurs in the mushy zone in the process of solidification, where the solid fraction is high[5]. Since 1940s, hot tearing has been widely investigated by metallurgists[6-8]. Generally, hot tearing is present in the interdendritic zone where the temperature is higher than solidus. It is noticeable that the three critical temperatures[9-12], i.e., coherence temperature, coalescence temperature and rigidity temperature, are closely related to the strength of the alloy during alloy solidification[13,14]. Coherence temperature is the temperature that the neighboring dendrites begin to interact and the granular solids form in the mushy zones; at this temperature, potential fractures can be healed by interdendritic feeding of surplus liquids and the tensile strength of the solid/liquid alloy mixture is still close to zero. Coalescence temperature is the temperature that the neighboring dendrites begin to coalesce or bridge; thus, the "solidus bridge" formed, and the tensile strength of the solid/liquid alloy mixture is dramatically enhanced. However, as the tensile strain increases continuously, the "solidus bridge" may be fractured, reducing tensile strength greatly and producing hot tearing if dendrites are not timely fed when lubricated by the liquid film. Rigidity temperature is the temperature that the continuous framework is formed in the dendrites, at which the solid is nearly fully occupying the alloy.

In the past decades, numerous experiments were designed to study the hot tearing susceptibility. Tears are usually generated due to the alloy contraction during solidification, which can be characterized by ring mould testing[15], cold finger testing[16] and backbone mould testing[17]. However, so far, the behavior and mechanism of hot tearing have not

* Corresponding author. Ph.D.
E-mail address: *cxr16@shu.edu.cn* (*X. R. Chen*).

Received 13 January 2017; Received in revised form 17 February 2017; Accepted 17 February 2016
Available online 15 April 2017

been well documented. Furthermore, the alloy's hot tearing behavior has been investigated through measuring the temperature, stress and strain during solidification, based on which some apparatuses have been developed. For example, the apparatus designed by Monroe and Beckermann[18] can explore the stress and strain of T-shaped casting during solidification; the double-sample hot tearing contraction device[19,20] can explore the stress and strain in one dimension. These devices quantitatively analyze the hot tearing behavior in alloys, which is beneficial to establishing the analysis model and criterion for hot tearing. Unfortunately, this kind of device is generally suitable for studying hot tearing behavior of nonferrous alloys. Even though the improved device could be used to study ferrous alloy, there is a large temperature gradient in the sample because of pouring and filling process, so it could not reflect the true shrinkage characteristic of ferrous alloy solidification process.

In the present study, hot tearing susceptibility of the DSS is investigated in an apparatus developed by the authors. In this apparatus, the huge temperature gradient during casting can be avoided, and the changes of temperature and stress during the solidification can be steadily and efficiently recorded respectively from two samples in the two cavities at the same time, which is conducive to more effectively quantitative analysis. It is common to test high-temperature mechanical properties of alloys using method of constrained solidification shrinkage in one dimension. Moreover, the study of the hot tearing susceptibility of ferrous alloy under in-situ solidification is rarely reported.

2. Experimental Devices and Methods

The composition of the DSS is listed in Table 1. The testing device is sketched in Fig. 1. This device is composed of a heating and argon protection system, a transmission system, and a data collection system. The sample was melted and held at 1560 ℃ for 5 min in the crucible fixed in the horizontal graphite holder. Then, the heating furnace moved quickly to the default location from the rail. The B-type thermocouple and test rod were inserted into the liquid immediately, with the test rod connected with a stress sensor. Data from the thermocouple and the stress sensor were collected by the data collection system. Metal liquids in this apparatus were protected by argon gas.

Table 1
Chemical composition of DSS (mass%)

C	Si	Mn	Cr	Ni	Mo	Cu	N	Fe
0.028	0.46	4.76	20.96	2.13	0.01	0.20	0.15	Balance

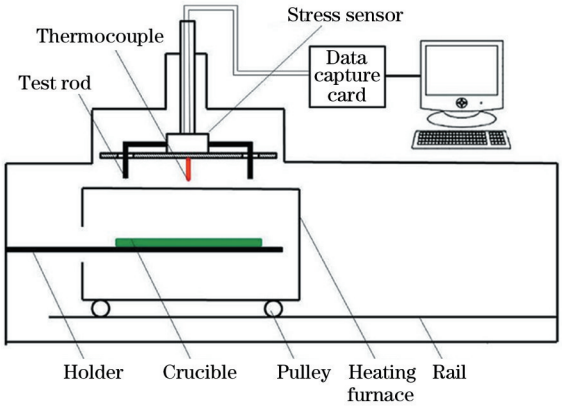

Fig. 1. Schematic diagram of the testing apparatus.

The crucible and testing points in the experiment are shown in Fig. 2. The Al_2O_3 crucible was kilned at high temperature. Because of the non-wettability between the material of crucible and molten steel, the friction force could be ignored. As shown in Fig. 2, there are two cavities in the crucible. To avoid interference from the thermocouple in the stress test, temperature and stress data were not obtained in one cavity; one cavity was used for testing stress during the free contraction of molten steel, and the other one was used for examining the temperature change. The liquid steel in the two cavities was melted and solidified in-situ at the same time. The data collected in the two cavities can be assumed as being simultaneous. The cavity is shown in Fig. 3. The distance between the two test rods, which are at both ends of the sample in direction of length, is 180 mm. This design is mainly to consider the generation of the contraction stress during the solidification shrinkage process in the length direction. When the free shrinkage in the length direction was constrained, the contraction stress during the solidification process could be tested by the two test rods at both ends of the sample. In the other cavity, the thermocouple lied in the center of the cross-section of

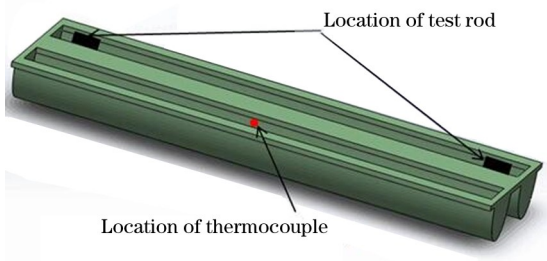

Fig. 2. Schematic diagram of the crucible.

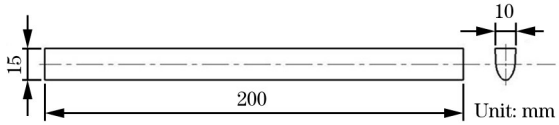

Fig. 3. Geometry of crucible cavity.